Dalton Transactions

Hard-Templating of Prussian Blue Analogues in Mesoporous Silica and Organosilica

Journal:	*Dalton Transactions*
Manuscript ID:	DT-ART-06-2015-002213.R1
Article Type:	Paper
Date Submitted by the Author:	16-Jul-2015
Complete List of Authors:	Wang, Pei-Xi; University of British Columbia, Dept. of Chemistry Zamarion, Vitor; University of British Columbia, Dept. of Chemistry Hamad, Wadood; FPInnovations, CNC-Biomaterials Group; UBC, Chemistry MacLachlan, Mark; UBC Chemistry, Chemistry Department

Journal Name

ARTICLE

Hard-Templating of Prussian Blue Analogues in Mesoporous Silica and Organosilica

Received 00th January 20xx,
Accepted 00th January 20xx

DOI: 10.1039/x0xx00000x

www.rsc.org/

Pei-Xi Wang,[a] Vitor M. Zamarion,[a,b] Wadood Y. Hamad[c] and Mark J. MacLachlan[a*]

ABSTRACT: Prussian blue analogues (PBAs) have been constructed in chiral nematic mesoporous organosilica and silica templates. By functionalizing the surface of the mesoporous hosts with bipyridinium ligands, it was possible to construct PBAs in their interiors through hard templating. The optical properties of the composites were studied and the relationship between the circular dichroism (CD) signals and the UV-Vis absorption spectra was found through mathematical modeling. Efforts to remove the hard templates to give free-standing PBA films with high surface area and pore volume were met with limited success, but it was possible in the case of zinc/iron PBAs to obtain a highly porous PBA sponge that retained the overall morphology of the template. This work demonstrates the potential for hard templating of coordination polymers in mesoporous materials.

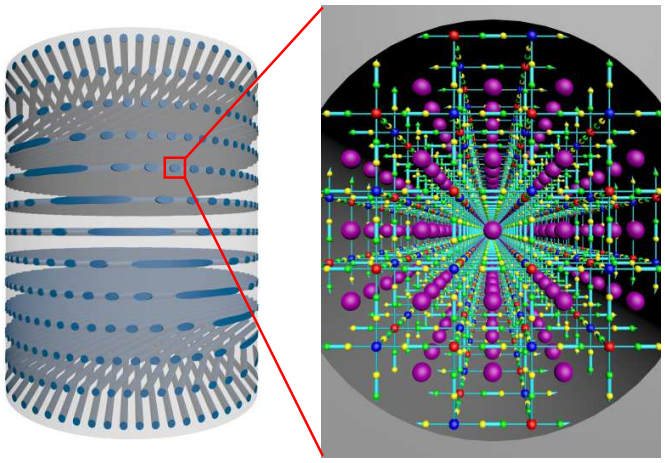

Introduction

There is a great deal of interest in the construction of inorganic/organic hybrid nanocomposites that combine the versatility of polymeric systems with the interesting properties of metal ions to produce new functional materials. In particular, coordination polymers[1,2,3] and metal-organic frameworks[4] have been able to unite physical and chemical properties of different organic/inorganic components for many applications, including catalysis,[3] separations, magnetism,[5,6] sensing[7,8,9] and gas storage.[10,11]

In this context, hard templating, also termed nanocasting, has emerged as a powerful synthetic method for constructing new nanostructured and especially mesoporous materials.[12] For this process, a well-defined template (e.g., mesoporous silica,[13] MCM-41) is used as the host to construct a hybrid material. After removal of the template, one is left with a nanostructured material that is a cast of the original porous host.[14] This method has been applied to diverse metal oxides,[15-18] carbon based materials[19-22] and other organic/inorganic materials.[23,24] Surprisingly, hard templating is virtually unexplored in the synthesis of metal-organic frameworks or other coordination polymers,[25] although extending the nanocasting method to coordination polymers may give new opportunities to

[a] *Department of Chemistry, University of British Columbia, 2036 Main Mall, Vancouver, British Columbia, Canada V6T 1Z1.*
Email: mmaclach@chem.ubc.ca
[b] *Departamento de Química Fundamental, Instituto de Química, Universidade de São Paulo, Av. Prof. Lineu Prestes, 748, cep 05508000, São Paulo, SP, Brazil.*
[c] *FPInnovations, 2665 East Mall, Vancouver, British Columbia, Canada V6T 1Z4.*
† Electronic Supplementary Information (ESI) available: additional figures, experimental data and simulation details. See DOI: 10.1039/x0xx00000x

form ordered porous materials with control over the metals and ligands.

Prussian blue (PB) is a metal-organic coordination framework of $Fe_4[Fe(CN)_6]_3 \cdot nH_2O$, where ions Fe^{3+} (high spin) and Fe^{2+} (low spin) occupy octahedral sites bridged by cyanide ligands. It has been used as a pigment for more than three hundred years,[26] where its intense blue color is dominated by an intervalence charge transfer transition between Fe^{2+} and Fe^{3+} sites.

Molecular complexes, generically represented by $M[Fe(CN)_5L]$, that represent a fragment of the PB lattice can be readily prepared. By changing the metal and donor-acceptor ligands L, the optical, magnetic and electrochemical properties of the complexes can be controlled.[27] When these complexes are combined with transition metal cations, such as Fe^{2+}, Cr^{3+}, Ni^{2+}, Cu^{2+}, or $Co^{2+/3+}$, the cyanide ligands can bridge the metal centers to form CN-M-NC bonds, thus forming an extended structure similar to Prussian blue, but integrating the ligand L.

As PB is the archetypical coordination polymer with fascinating properties, many efforts have been reported to form nanostructured Prussian blue[28 - 32] as well as its analogues.[33 - 36] For example, templating with block copolymers and lyotropic liquid crystal surfactants has been applied to the synthesis of mesoporous and nanostructured PB and PB analogues.[37,38] Nanocasting has, however, not yet been applied to the PB family of materials.

In this paper, we describe our efforts to construct mesoporous chiral silica/PB composite materials using a tethered ligand approach. Removal of the silica led to degradation of the material in many cases, but we were successful in obtaining the first PB analogue composites with a chiral superstructure by this method.

Experimental section

Preparation of Chiral Nematic Mesoporous Silica and Organosilica Films

Chiral nematic mesoporous silica[39] and ethylene-bridged organosilica[41] were prepared according to literature procedures. In this study CNC suspensions (4 wt% in water, pH 2.14) prepared by H_2SO_4 hydrolysis of wood pulp were used as chiral nematic liquid crystal templates.[40] (The CNCs were provided by CelluForce, and TEM analysis showed that they have lengths of 195 ± 93 nm and widths of 15 ± 8 nm.) In a typical procedure, 1 mL (4 mmol) 1,2-bis(trimethoxysilyl)ethane (BTMSE) or 1.56 mL (10.5 mmol) tetramethoxysilane (TMOS) was mixed with 30 mL CNC suspension (~1.2 g CNCs) to form a homogeneous suspension after stirring for 5 h at room temperature, which was then poured into polystyrene Petri dishes and dried under ambient conditions. Cellulose in the resulting CNC-organosilica or CNC-silica composite films was removed by hydrolysis in 6 M sulfuric acid at 100 °C for 24 h, followed by complete removal of cellulosic hydrolysis byproducts and activation of the pore surface in piranha solution (4:1 H_2SO_4/H_2O_2) for 2 h, then washed by deionized water and dried.

Functionalization of Silica and Organosilica Films

Organosilica or silica films (500 mg) were put into 20 mL anhydrous toluene containing 1 mL (5.1 mmol) (3-iodopropyl)trimethoxysilane (ITS) and heated to 95 °C under nitrogen for 60 h. After that, the films were isolated by filtration and were washed 5 times alternately with each of toluene and acetonitrile. The films were then placed in 20 mL acetonitrile containing 750 mg (4.8 mmol) 4,4'-bipyridine (BiPy) and the system was heated to 65 °C for 48 h. Residual bipyridine was removed by washing with ethanol, then the films were dried at ambient conditions. After drying, the BiPy-modified films were treated with 0.1 M $Na_3[Fe(CN)_5NH_3]$ aqueous solution for 48 h, then washed with deionized water and dried in air.

Deposition of Multilayer Prussian Blue Analogues

A piece of BiPy-modified film obtained in the last step was first immersed in the appropriate aqueous solution of $FeCl_3$ (0.01 $mol \cdot L^{-1}$) + KCl (0.5 $mol \cdot L^{-1}$) (pH = 2 adjusted by HCl), or $Zn(NO_3)_2$ (0.01 $mol \cdot L^{-1}$) + KCl (0.5 $mol \cdot L^{-1}$), for 30 min. Then, the films were briefly rinsed with deionized water in three separate beakers to remove residual absorbed solution, immersed in $K_4[Fe(CN)_6]$ (0.01 $mol \cdot L^{-1}$) + KCl (0.5 $mol \cdot L^{-1}$) aqueous solution for another 30 min, and cleaned 3 times with deionized water again. Thus a layer of Prussian blue analogue had been deposited onto the surface of the internal pores of the film. The process described above was repeated 10 times to form multilayer Prussian blue analogues (PBAs) with increased thickness inside the hard template until the pores and channels were completely filled.

Removal of the Organosilica or Silica Templates

Since PB is known to be unstable in base, we tried three different hydrofluoric acid solutions to remove hard templates from those composite films: 2 wt% HF aqueous solution, 2 wt% HF aqueous solution with $K_4[Fe(CN)_6]$ (0.2 $mol \cdot L^{-1}$) + K_2SO_4 (0.2 $mol \cdot L^{-1}$), and 2 wt% HF ethanol solution. The etching time selected for PBA@Silica films was 1 h, while for PBA@Organosilica films the etching time was 12 h. All experiments were conducted at room temperature without heating or stirring. After etching in aqueous HF solution the samples were carefully washed with a copious amount of deionized water to remove water soluble salts and residual HF, then water was removed by solvent exchange with ethanol and supercritical drying. When HF ethanol solution was used as an etchant, the films were washed several times with fresh ethanol to remove HF acid after etching, and finally dried by supercritical CO_2.

Results and discussion

CNCs were prepared from hydrolysis of kraft wood pulp in sulfuric acid.[40] Mesoporous organosilica[41] and silica[39] films with chiral nematic ordering were obtained through previously reported methods. Briefly, 1,2-bis(trimethoxysilyl)ethane (BTMSE) or tetramethoxysilane (TMOS) was added to an aqueous suspension of CNCs to form a homogeneous mixture after stirring, which was then poured into polystyrene Petri dishes and dried at room temperature. The resulting CNC-organosilica or CNC-silica composite films were heated in sulfuric acid to hydrolyze CNCs, followed by piranha solution washing to remove residual polyfurans. Nitrogen adsorption measurements showed that the organosilica and silica films prepared in this way had surface areas of 535 and 330 m^2/g, and pore dimensions of about 9.3 and 10.7 nm, respectively (Table 1 & Figure S1). IR spectroscopy confirmed removal of cellulose from the films.

The piranha solution treatment also activated the surface of the silica and organosilica films obtained, raised the density of Si-OH groups that would facilitate the surface functionalization with ITS in the next step, which was conducted according to a recently reported method.[42] Then BiPy was introduced by replacing the alkyl iodide groups through a nucleophilic substitution reaction, resulting in dark orange films that were named as **OrgSi-BiPy** or **Silica-BiPy** according to the templates used. The presence of BiPy in the films was confirmed by FTIR spectroscopy (Figure 1e & Figure 2e), which showed characteristic bands at 1465 cm^{-1} (ν_{ring} + δ_{CH}) and 1640 cm^{-1} (ν_{ring}).[43, 44] Thus, the chiral nematic mesoporous organosilica and silica have a thin film of bipyridinium on the surface of the pores. Elemental analysis of 2 samples of BiPy-modified silica films gave a surface coverage of ~1.2-1.4 BiPy nm^{-2} (See ESI for more information).

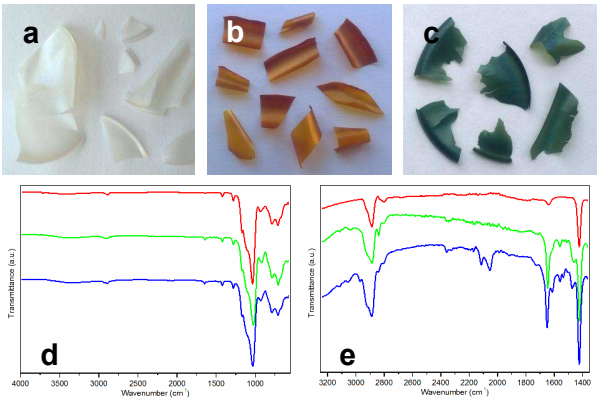

Figure 1. Photographs of (a) chiral nematic mesoporous organosilica films, (b) **OrgSi-BiPy**, and (c) **OSBP-FeCmp**. (d) FTIR spectra of organosilica films (red curve), **OrgSi-BiPy** (green curve), and **OSBP-FeCmp** (blue curve). An expanded view of the same spectra in the region of 1400-3200 cm^{-1} is shown in (e).

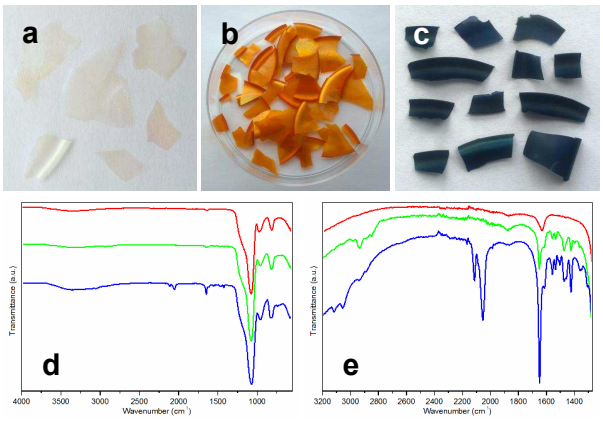

Figure 2. Photographs of (a) chiral nematic mesoporous silica films, (b) **Silica-BiPy**, and (c) **SiBP-FeCmp**. (d) FTIR spectra of silica films (red curve), **Silica-BiPy** (green curve), and **SiBP-FeCmp** (blue curve). An expanded view of the same spectra in the region of 1400-3200 cm^{-1} is shown in (e).

To fill the channels of the **OrgSi-BiPy** or **Silica-BiPy** films with Prussian blue analogues, a layer of ferrocyanide complex must be tethered onto the surface of the channels and pores before PBA can be formed. Alkylbipyridinium species are known to be good ligands for pentacyanoferrate(II) complexes.[45,46] Thus, the organosilica and silica films **OrgSi-BiPy** or **Silica-BiPy** with tethered bipyridinium ligands were treated with an aqueous solution of $Na_3[Fe(CN)_5NH_3]$. There was a rapid color change from dark orange to dark green, indicating the formation of a $[BiPy\text{-}Fe(CN)_5]^{3-}$ layer inside the films. FTIR spectroscopy (Figure 1 & Figure 2) also showed the characteristic CN stretching bands at 2051 and 2112 cm^{-1}, indicating that $[Fe(CN)_5L]^{3-}$ groups were incorporated into the films and were attached to the bipyridinium ligands. For comparison, the CN stretching bands for $Na_3[Fe(CN)_5NH_3]$ are observed at 2032 and 2044 cm^{-1}. There is a splitting of the CN bands due to the low molecular symmetry, which was notably enhanced by the BiPy ligands. These films functionalized with $[Fe(CN)_5L]^{3-}$ groups were named as **OSBP-FeCmp** or **SiBP-FeCmp**. The functionalization process is depicted in Figure 3.

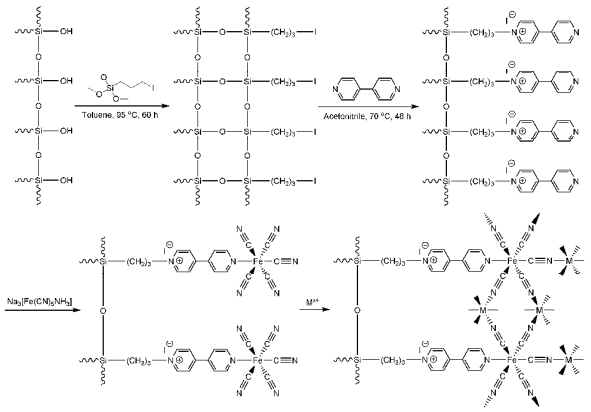

Figure 3. Functionalization process of chiral nematic mesoporous organosilica and silica films.

In order to confirm that the functionalization of the organosilica and silica templates happened not only on the outer surface, cross-sections of the materials were imaged at each stage of functionalization. Freshly cleaved edges of chiral nematic organosilica, **OrgSi-BiPy**, **OSBP-FeCmp** and monolayer **OSFeFe** films were photographed (Figure S2). (Monolayer **OSFeFe** films were made by immersing **SiBP-FeCmp** films once in 0.01 M $FeCl_3$ + 0.5 M KCl aqueous solution for 30 min, then washing them with deionized water to remove residual absorbed solution.) In each case, it is clear that the coloration is homogeneous throughout the thickness of the film and not localized on the outer surfaces.

The extended Prussian blue analogues (PBAs) were assembled on the surface of the pores inside the hard templates through a sequential deposition process, similar to that which has been used for making PBA membranes on substrates.[47, 48] In brief, the functionalized organosilica or silica films with a single layer of

$[BiPy\text{-}Fe(CN)_5]^{3-}$ were consecutively immersed into an aqueous solution of Fe^{3+} or Zn^{2+} (M^{x+}), deionized water, an aqueous solution of $[Fe(CN)_6]^{4-}$ and deionized water again, denoted as a four-step cycle in Diagram S1.

Ideally the thickness of the PBA layer would increase by about 1 nm as the lattice parameters of PBAs are commonly in the range of 10-11 Å.[49,50] In theory, the pores of the hard templates we have employed, which are generally about 8 nm in diameter, would be filled after 4 cycles.

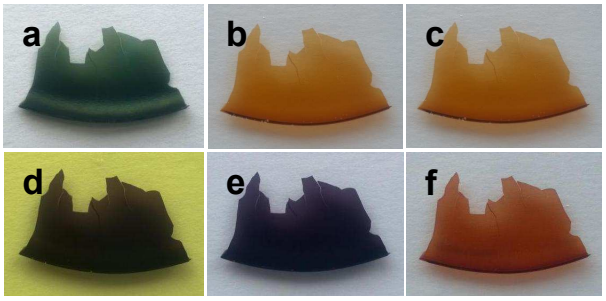

Figure 4. A piece of **OSBP-FeCmp** film (a), successively treated with $Zn(NO_3)_2$ + KCl solution (b), deionized water (c), $K_4[Fe(CN)_6]$ + KCl solution (d), deionized water (e), and $Zn(NO_3)_2$ + KCl solution again (f).

Interestingly, the color of the films changed dramatically during deposition cycles, allowing for visual monitoring of the reaction progress. Films with a single monolayer of $[BiPy\text{-}Fe(CN)_5]^{3-}$ were initially dark green, but they turned pink when they were immersed into Zn^{2+} solution. After washing with deionized water, the films were put into $[Fe(CN)_6]^{3-}$ solution and became dark violet. Upon immersion into Zn^{2+} solution, the films reverted to a pink color, although darker than the first time, as shown in Figure 4. This color alternation ended after 5 to 6 cycles with a dark purplish red color that did not change further, consistent with fully filling the channels of the material. In this study the deposition was repeated for 15 cycles to ensure a large loading amount of PBA, and thus a highly cross-linked network. The resulting PBA@Organosilica or PBA@Silica composite films were named as **OSFeFe**, **OSFeZn**, **SiFeFe**, or **SiFeZn** according to the film and transition metal salt used. In a typical procedure, from 116.4 mg chiral nematic mesoporous silica films, 168.9 mg **SiFeZn** composites could be made, which contained 31.1 wt% zinc PBA inside, and the existence of iron and zinc was confirmed by energy dispersive X-ray (EDX) analysis (Table S1).

The existence of zinc PBA in **SiFeZn** composite films was confirmed by powder X-ray diffraction (PXRD) as the pattern was perfectly consistent with that of $Zn_2Fe(CN)_6{\cdot}3H_2O$ (Figure S3). The FTIR spectra showed strong bands at 2096 cm^{-1} (ν_{CN}) and 599 cm^{-1} (ν_{FeC}) indicating that zinc PBA had been loaded into the films (Figure 8c), which is consistent with the spectrum of zinc PBA prepared from solution without templates (Figure S8b), and the data from the literature.[51] As a result of higher molecular symmetry, the splitting of the CN stretching bands of $[Fe(CN)_5L]^{3-}$ groups disappeared after PBA loading. In addition, a significant decrease in BET surface area and pore volume from silica template films to **SiFeZn** composites was also revealed by N_2 adsorption measurements (Figure 8d & Table 1). Scanning electron microscopy (SEM) images of **SiFeZn** films (Figure 5) clearly show the characteristic chiral nematic structure originating from CNCs, which proved the chiral arrangement of Prussian blue analogues inside the pores and channels of these materials.

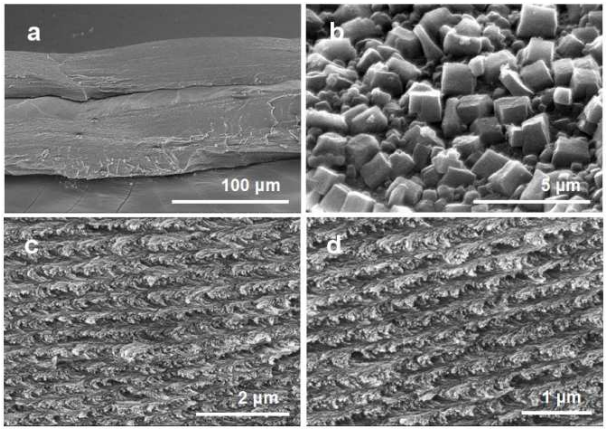

Figure 5. SEM images of **SiFeZn** composite films. (a) Side view of a cracked film. The twisted layered structure of chiral nematic mesoporous silica is evident in the images (c,d) of higher magnification. (b) Top view of a film shows PBA microcrystals on its outer surface.

There has been a great deal of interest in materials with chiroptical properties for applications in sensing and photonics. Many researchers have been investigating how chiral environments can influence the chirality of guests and their spectroscopy by both experimental and theoretical methods.[52,53] The combination of strong CD signals from the chiral nematic superstructure and the various colors of the PBAs offers a good opportunity to explore chiroptical effects in these composites.

To study the influence of the loaded PBAs on the CD signals from the chiral nematic structure, a series of monolayer PBA@Silica composite films (Figure S4) was prepared. Silica matrices were selected for these samples as they are much more rigid than organosilica, thus the helical pitch of the hard templates would not be significantly changed during the functionalization process. At first, **Silica-BiPy** and **SiBP-FeCmp** films were successively prepared from the same batch of chiral nematic mesoporous silica films, UV-Vis and CD spectra of these materials were then measured and compared as shown in Figure 6a. The CD signal of the original silica template closely matched with its UV-Vis reflectance peak, while for the composites with BiPy or $[BiPy\text{-}Fe(CN)_5]^{3-}$, their CD spectra seemed to be reshaped by the strong UV-Vis absorption, which was further revealed by the study of PBA@Silica composite films.

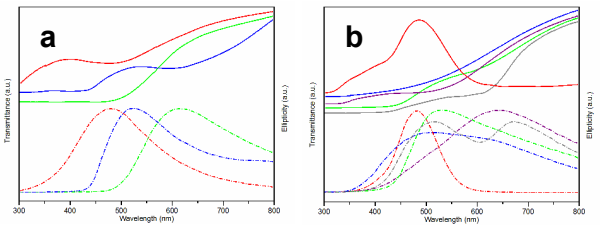

Figure 6. UV-Vis transmittance spectra (Solid curves) and CD spectra (dashed curves) of different films: chiral nematic mesoporous silica (a, red curve); **Silica-BiPy** (a, green curve); **SiBP-FeCmp** (a, blue curve); **SiFeFe** (b, Red curve); **SiFeCo** (b, gray curve); **SiFeNi** (b, green curve); **SiFeSn** (b, blue curve) and **SiFeZn** (b, purple curve).

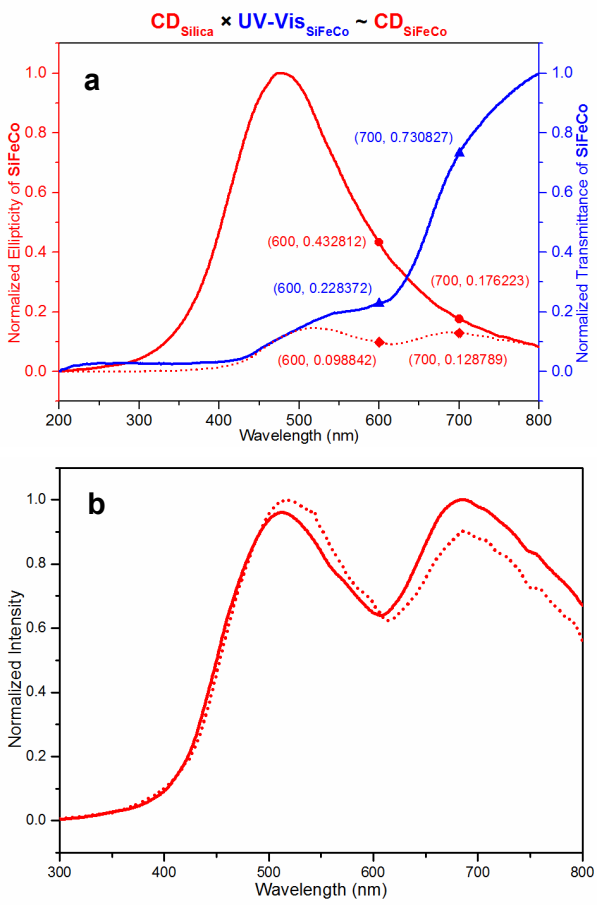

Figure 7. (a) Normalized CD spectrum of pristine silica film (red solid curve) and normalized UV-Vis transmittance spectrum of **SiFeCo** composite film (blue curve). The product of them is shown as a red dotted curve, which resembles the CD spectrum of **SiFeCo** (simulated CD signals). (b) Simulated CD signals of **SiFeCo** (dotted curve) compared with a real CD spectrum of it (solid curve). Both of them are normalized between 0 and 1.

SiBP-FeCmp films from the same batch as the ones described above were used to prepare PBA@Silica composite films by immersing them once in 1 mol·L^{-1} $Fe(NO_3)_3$, $CoCl_2$, $NiCl_2$, $SnCl_2$ or $Zn(NO_3)_2$ aqueous solutions, then they were washed by deionized water and dried, leaving one layer of PBA deposited onto the surface of the pores inside the films. These films all showed unique CD spectra that were completely different from the CD spectrum of the silica template (Figure 6b), and the CD signals of **SiFeCo** and **SiFeSn** even showed two bands. It seemed impossible to us that embedding only one layer of PBA in the silica could change the helical pitch of the hard template. To verify this hypothesis, we carefully treated a piece of **SiFeCo** film with 0.5 M $NaOH_{(aq)}$ for 5 min at room temperature to degrade the cobalt PBA without dissolving the whole film, then washed it with deionized water. When the CD measurement was conducted again on the dried film, it showed a reflection at nearly the same wavelength as the parent **SiBP-FeCmp** film as shown in Figure S5, verifying that the helical pitch of the silica template was not changed.

We speculated that the CD signals of the silica templates were reshaped by the strong UV-Vis absorption of the PBAs, and we therefore modeled this mathematically. Here the CD signals of a chiral nematic silica template and a PBA@Silica composite film (**SiFeM**, M = Fe, Co, Ni, Sn, Zn) are defined as $g_1(\lambda)$ and $g_2(\lambda)$, respectively, while the UV-Vis transmittance spectra of them are defined as $f_1(\lambda)$ and $f_2(\lambda)$, respectively. At first we thought there should be a relationship between them as $g_1(\lambda)\times f_2(\lambda)/f_1(\lambda) = g_2(\lambda)$, because in Figure 6b when the UV-Vis transmittance of a PBA@Silica composite film became zero, its CD spectrum went to zero at the same wavelength (as shown by the spectra of **SiFeNi**). If instead the UV-Vis transmittance was not zero in the range of 450-500 nm, there would also be a strong CD peak matching that of the parent silica template, as shown by the curves of **SiFeFe** and **SiFeCo**. Finally, we found that the product of $g_1(\lambda)$ and $f_2(\lambda)$ dramatically resembled the CD spectra of the corresponding PBA@Silica composite films, which meant $\mathbf{N}[g_2(\lambda)] = \mathbf{N}\{\mathbf{N}[g_1(\lambda)]\times\mathbf{N}[f_2(\lambda)]\}$ as shown in Figure 7. Here a 0 to 1 normalization operator $\mathbf{N}(A)$ of (x-Min)/(Max-Min) is used, where A is a set of real numbers, x is an element of A, while Min and Max represent the minimum and maximum of all the elements, respectively (see full explanation in the Supporting Information).

Thus it seemed the UV-Vis signals of the chiral nematic silica films was negligible if compared with the strong absorption of PBAs. The CD peaks of PBA@Silica composites in fact originated from the "background" CD signals of the silica templates, which were reshaped by the strong selective absorption of the PBAs to give unique patterns; the PBAs inside the chiral nematic films just worked as "optical filters" and did not show their own CD signals even though they were arranged in a chiral environment. These results may be applicable to other materials in chiral nematic liquid crystals and solids with chiral nematic order, and one should be cautious of the interpretation of this data – CD signals observed in some cases may arise from reshaping of the background CD signal of the chiral matrix by the UV-Vis absorption of the guest, rather than from a distinct CD signal of the guest itself.[54-58] We note that we had already analyzed this data and had grown skeptical of the origin of CD signals in chiral nematic metal nanoparticle and nanorod composites when Prof. Kumacheva at the University of Toronto mentioned that they also had simultaneously unearthed the same results in related systems.

Our intention was to remove the silica or organosilica template to reveal a porous PB network with chiral nematic order. This turned out to be much more difficult than we expected! In order to obtain nanostructured bulk Prussian blue analogue materials, a number of attempts were made to remove hard templates from these composite films. As almost all PBAs are sensitive to base due to the insolubility of transition metal hydroxides, hydrofluoric acid was selected as the reagent of choice for removing silica and organosilica templates from the composite films.

Previous tests showed that organosilica films needed more than 6 h to be thoroughly dissolved by 2 wt% HF aqueous solution. However, when we tried to remove hard templates from PBA@organosilica composite films under the same conditions, only a clear blue solution (**OSFeFe**) or pale green amorphous powder (**OSFeZn**) was obtained after etching. It seemed the PBA network formed within the organosilica template was insufficiently robust to obtain a freestanding film. We postulate that the higher hydrophobicity and lower surface hydroxyl group density that arise from the ethylene bridging groups of organosilica templates impede the condensation of ITS, and finally resulted in a lower PBA loading amount with insufficient interconnectivity.

Interestingly, in the presence of $K_4[Fe(CN)_6]$ and K_2SO_4, brittle films could finally be obtained after etching, but it seemed the PBAs had been chemically destroyed as the strong IR band of cyano groups at around 2080-2090 cm^{-1} disappeared after etching, while the strong stretching vibration band of Si-O-Si in the range of 1000-1300 cm^{-1} were still present. In addition, a new peak arose at about 743 cm^{-1}, which could not be attributed to either $K_4[Fe(CN)_6]$ or K_2SO_4 (Figure S6); although we cannot verify the origin of this peak, it may be due to fluorosilicates. Clearly, chiral nematic organosilica films may not be good templates for preparing free-standing nanostructured PBAs in this way, but the composite material is still an interesting one, since according to our knowledge, it is the first example in the literature where a chiral PBA was synthesized.

We also investigated template removal from the PBA@Silica composites. **SiBP-FeCmp** films could be completely etched by 2 wt% $HF_{(aq)}$ solution in 20 min, leaving only a trace amount of brown powder due to the Fe(II) ions contained. In 2 wt% HF/ethanol solution, 60 min were needed to decompose the silica template from **SiBP-FeCmp**, leaving a highly shrunk and curled soft green film, which might include fluorosilicates that were insoluble in ethanol. **SiFeFe** films quickly dissolved in aqueous HF, resulting in a clear blue solution. However, in the presence of $K_4[Fe(CN)_6]$ and K_2SO_4, intact dark blue films were finally obtained (Figure S7). The removal of silica as well as the preservation of Prussian blue could be confirmed by FTIR spectra, which showed strong peaks at 2068 cm^{-1} (ν_{CN}) and 594 cm^{-1} (ν_{FeC}) indicating the presence of PB, while the stretching vibration band of Si-O-Si at around 1068 cm^{-1} disappeared. The unassigned peak at 743 cm^{-1} was again present in these samples (Figure S7c), which could not be explained by either $K_4[Fe(CN)_6]$ or K_2SO_4 (Figure S8a). In addition, SEM images of the dark blue product indicated that the Prussian blue had recrystallized into randomly arranged big crystals, thus losing any chiral superstructure imparted by the chiral nematic template (Figure S7d,e).

On the other hand, zinc Prussian blue analogue showed uniquely high stability in HF. After etching in 2 wt% $HF_{(aq)}$ solution for 1 h, the films became brittle, shrunk, broke into small pieces upon drying in air. The integrity of those films could only be kept by supercritical drying, which gave light purple to dark red free-standing films depending on the PBA loading amount (Figure 8b). In a typical procedure, 33.2 mg zinc PBA could be obtained from 168.9 mg **SiFeZn** composites after HF etching. Complete removal of silica was confirmed by FTIR spectra (Figure 8c), while PXRD analysis proved that the zinc PBA was well preserved (Figure S3). EDX (Figure S9 & Table S1) also showed a sharp decrease in silicon and oxygen after HF etching, which was accompanied by a significant increase of iron and zinc. These samples were named as **SiZnHF**.

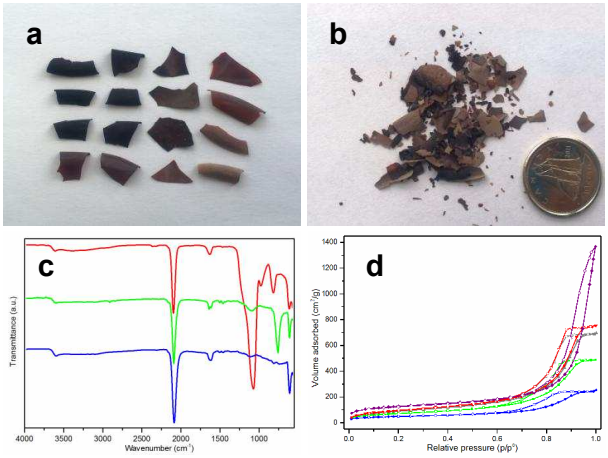

Figure 8. Photographs of (a) **SiFeZn** composite films, and (b) after etching in 2 wt% HF aqueous solution for 60 min. (c) FTIR spectra of **SiFeZn** (red curve) after HF etching in water (blue curve) or ethanol (green curve). (d) N_2 adsorption/desorption isotherms of chiral nematic mesoporous silica templates (red curve), **Silica-BiPy** (gray curve), **SiBP-FeCmp** (green curve), **SiFeZn** (blue curve), and **SiZnHF** (purple curve).

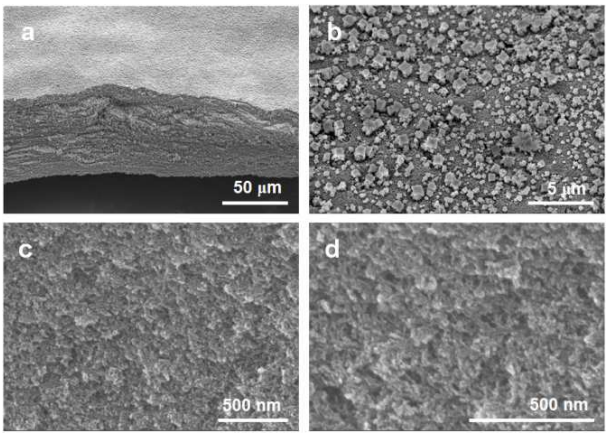

Figure 9. SEM images of **SiZnHF** films. (a) Side view of a cracked film, images of higher magnification (c,d) illustrate

loss of chirality in the loose porous PBA sponge. (b) Top view of a film.

The films were not homogeneous due to the nature of Prussian blue analogues themselves. In most cases the PBA network looked like a loose and porous sponge with a degraded layered structure without chirality as shown in Figure 9, but in some regions there are highly porous aerogels made up of nanofibrils with a diameter of about 10 nm (Figure S10).

HF/ethanol solution was a mild etchant that could slowly break the silicon-oxygen bonds of the silica matrix, leaving insoluble fluorosilicates that showed a strong IR peak at about 760 cm^{-1} (Figure 8c). The slower etching rate in HF/ethanol solution helped to keep the superstructure of the PBAs when the silica matrix was removed, but long soaking times (e.g., 14 h) in this etchant caused significant reconstruction of the PBAs and yielded large crystals with a peach kernel shape (Figure S11). This unfavorable phenomenon did not occur in aqueous HF solution.

Table 1. Nitrogen adsorption data of silica composite films at different stages.

Sample	BET Surface Area (m^2/g)	Micropore Area (m^2/g)[a]	Pore Volume (cm^3/g)[b]	Pore Size (nm)[c]
Silica	347	N/A	1.16	11.3
Silica-BiPy	330	N/A	1.05	10.7
SiBP-FeCmp	255	6	0.75	10.1
SiFeZn	163	29	0.38	9.4
SiZnHF	457	49	2.23	19.8

[a] Calculated by t-plot analysis from the adsorption branches.
[b] BJH (Barrett-Joyner-Halenda model) Adsorption cumulative pore volume.
[c] BJH Adsorption average pore width (4V/A).

The porosity of those samples at each modification stage was measured through nitrogen adsorption/desorption studies (Figure 8d and Table 1). All four samples showed type IV isotherms with significant H1 hysteresis loops, which indicated that they were mesoporous. The average pore size did not change too much from **SiBP-FeCmp** to **SiFeZn** after PBA loading, but the obvious decrease of cumulative pore volume suggested pore blocking or inefficient and uneven filling due to the crystallization property of PBAs. This also explained why the chiral nematic structure of the hard template was not retained after HF etching, as the weaker branches of the PBA network would be broken when silica was etched.

After removal of the hard template, **SiZnHF** showed much higher surface area and pore volume partly due to the lower density of zinc PBA compared with silica, and the pore size significantly increased to 20 nm, which represented the wall thickness of the silica matrix. Thus, we were able to obtain a mesoporous PBA material by our novel hard templating method.

Conclusions

In summary, we have prepared free-standing nanostructured Prussian blue analogues through hard-templating in chiral nematic mesoporous organosilica and silica films. It was possible to construct Prussian blue analogues within the channels of the mesoporous template by a stepwise procedure that afforded PBA/silica composites with retention of chiral nematic order. Although CD signals were apparent for these materials, mathematical modeling demonstrated that the unique CD patterns of these composites actually arise from reshaping of the CD spectra of the hard templates, while the PBAs in the chiral environment do not show their own CD signals.

Removal of the hard template proved challenging, especially for the organosilica hard templates. Nevertheless, we succeeded in removing the silica template in the case of chiral nematic mesoporous **SiFeZn**, and obtained a freestanding mesoporous PBA material. Our approach may be adapted to other forms of silica and other PBAs. Given the wide range of fascinating magnetic, optical, electronic, and catalytic properties of PBAs with different metals, we hope that our results will help to guide the development of new materials.

Acknowledgements

This project was supported by the Natural Sciences and Engineering Research Council (NSERC) of Canada. We thank FPInnovations and CelluForce for support. P.X.W. is grateful to UBC for a 4YF graduate fellowship.

References

(1) I. Manners, *Science* **2001**, *294*, 1664–1666.
(2) G. R. Whittell and I. Manners, *Adv. Mater.* **2007**, *19*, 3439–3468.
(3) S. Kitagawa, R. Kitaura and S. Noro, *Angew. Chem. Int. Ed. Engl.* **2004**, *43*, 2334–2375.
(4) D. Bradshaw, J. B. Claridge, E. J. Cussen, T. J. Prior and M. J. Rosseinsky, *Acc. Chem. Res.* **2005**, *38*, 273–282.
(5) S. Ferlay, T. Mallah, R. Ouahès, P. Veillet and M. Verdaguer, *Nature* **1995**, *378*, 701–703.
(6) M. Ohba and H. Ōkawa, *Coord. Chem. Rev.* **2000**, *198*, 313–328.
(7) O. Kahn and C. J. Martinez, *Science* **1998**, *279*, 44–48.
(8) S. W. Thomas, G. D. Joly and T. M. Swager, *Chem. Rev.* **2007**, *107*, 1339–1386.
(9) G. J. Halder, C. J. Kepert, B. Moubaraki, K. S. Murray and J. D. Cashion, *Science* **2002**, *298*, 1762–1765.
(10) L. J. Murray, M. Dincă and J. R. Long, *Chem. Soc. Rev.* **2009**, *38*, 1294–1314.
(11) J. L. C. Rowsell and O. M. Yaghi, *Angew. Chem. Int. Ed. Engl.* **2005**, *44*, 4670–4679.
(12) A.-H. Lu and F. Schüth, *Adv. Mater.* **2006**, *18*, 1793–1805.

(13) S.-H. Wu, C.-Y. Mou and H.-P. Lin, *Chem. Soc. Rev.* **2013**, *42*, 3862–3875.
(14) M. Giese, L. K. Blusch, M. K. Khan, W. Y. Hamad and M. J. MacLachlan, *Angew. Chem. Int. Ed. Engl.* **2014**, *53*, 8880–8884.
(15) K. E. Shopsowitz, A. Stahl, W. Y. Hamad and M. J. MacLachlan, *Angew. Chem. Int. Ed. Engl.* **2012**, *51*, 6886–6890.
(16) A. Rumplecker, F. Kleitz, E.-L. Salabas and F. Schüth, *Chem. Mater.* **2007**, *19*, 485–496.
(17) H. Kim and J. Cho, *J. Mater. Chem.* **2008**, *18*, 771–775.
(18) X. Lai, G. Shen, P. Xue, B. Yan, H. Wang, P. Li, W. Xia and J. Fang, *Nanoscale* **2015**, *7*, 4005–4012.
(19) R. Ryoo, S. H. Joo and S. Jun, *J. Phys. Chem. B* **1999**, *103*, 7743–7746.
(20) J. Lee, S. Yoon, T. Hyeon, S. M. Oh and K. Bum Kim, *Chem. Commun.* **1999**, 2177–2178.
(21) T.-D. Nguyen and M. J. MacLachlan, *Adv. Opt. Mater.* **2014**, *2*, 1031–1037.
(22) R. Silva, D. Voiry, M. Chhowalla and T. Asefa, *J. Am. Chem. Soc.* **2013**, *135*, 7823–7826.
(23) Y.-S. Jun, W. H. Hong, M. Antonietti and A. Thomas, *Adv. Mater.* **2009**, *21*, 4270–4274.
(24) G. Chu, J. Feng, Y. Wang, X. Zhang, Y. Xu and H. Zhang, *Dalton Trans.* **2014**, *43*, 15321–15327.
(25) T. Ishiwata, Y. Furukawa, K. Sugikawa, K. Kokado and K. Sada, *J. Am. Chem. Soc.* **2013**, *135*, 5427–5432.
(26) L. J. M. Coleby, *Ann. Sci.* **1939**, *4*, 206–211.
(27) H. E. Toma and J. M. Malin, *Inorg. Chem.* **1973**, *12*, 2080–2083.
(28) S. Vaucher, M. Li and S. Mann, *Angew. Chem. Int. Ed. Engl.* **2000**, *39*, 1793–1796.
(29) P. Zhou, D. Xue, H. Luo and X. Chen, *Nano Lett.* **2002**, *2*, 845–847.
(30) G. Liang, J. Xu and X. Wang, *J. Am. Chem. Soc.* **2009**, *131*, 5378–5379.
(31) X.-J. Zheng, Q. Kuang, T. Xu, Z.-Y. Jiang, S.-H. Zhang, Z.-X. Xie, R.-B. Huang and L.-S. Zheng, *J. Phys. Chem. C* **2007**, 111, 4499–4502.
(32) N. L. Torad, M. Hu, M. Imura, M. Naito and Y. Yamauchi, *J. Mater. Chem.* **2012**, *22*, 18261–18267.
(33) E. Dujardin and S. Mann, *Adv. Mater.* **2004**, *16*, 1125–1129.
(34) M. Cao, X. Wu, X. He and C. Hu, *Chem. Commun.* **2005**, 2241–2243.
(35) H.-L. Sun, H. Shi, F. Zhao, L. Qi and S. Gao, *Chem. Commun.* **2005**, 4339–4341.
(36) X. Wu, M. Cao, C. Hu and X. He, *Crystal Growth & Design* **2006**, *6*, 26–28.
(37) X. Roy, J. K.-H. Hui, M. Rabnawaz, G. Liu and M. J. MacLachlan, *J. Am. Chem. Soc.* **2011**, *133*, 8420–8423.
(38) X. Roy, J. K.-H. Hui, M. Rabnawaz, G. Liu and M. J. MacLachlan, *Angew. Chem. Int. Ed. Engl.* **2011**, *50*, 1597–1602.
(39) K. E. Shopsowitz, H. Qi, W. Y. Hamad and M. J. MacLachlan, *Nature* **2010**, *468*, 422–425.
(40) W. Y. Hamad and T. Q. Hu, *Can. J. Chem. Eng.* **2010**, *88*, 392–402.
(41) K. E. Shopsowitz, W. Y. Hamad and M. J. MacLachlan, *J. Am. Chem. Soc.* **2012**, *134*, 867–870.
(42) J. Min, Y. Lin, J. Zheng and T. Tang, *Chem. Commun.* **2015**, *51*, 5921–5924.
(43) E. B. Wilson, *Phys. Rev.* **1934**, *45*, 706–714.
(44) B. Hennessy, S. Megelski, C. Marcolli, V. Shklover, C. Bärlocher and G. Calzaferri, *J. Phys. Chem. B* **1999**, *103*, 3340–3351.
(45) H. E. Toma and J. M. Malin, *Inorg. Chem.* **1973**, *12*, 2080–2083.
(46) H. E. Toma and J. M. Malin, *Inorg. Chem.* **1973**, *12*, 1039–1045.
(47) W. Jin, A. Toutianoush, M. Pyrasch, J. Schnepf, H. Gottschalk, W.Rammensee and B. Tieke, *J. Phys. Chem. B* **2003**, *107*, 12062–12070.
(48) J. T. Culp, J.-H. Park, I. O. Benitez, Y.-D. Huh, M. W. Meisel and D. R. Talham, *Chem. Mater.* **2003**, *15*, 3431–3436.
(49) D. B. Brown and D. F. Shriver, *Inorg. Chem.* **1969**, *8*, 37–42.
(50) A. Ludi and H. Güdel, *Inorg. Chem.* **1973**, *14*, 1–21.
(51) S. N. Ghosh, *J. Inorg. Nucl. Chem.* **1974**, *36*, 2465–2466.
(52) E. Sackmann and J. Voss, *Chem. Phys. Lett.* **1972**, *14*, 528–532.
(53) F. D. Saeva, P. E. Sharpe and G. R. Olin, *J. Am. Chem. Soc.* **1973**, *95*, 7656–7659.
(54) H. Qi, K. E. Shopsowitz, W. Y. Hamad and M. J. MacLachlan, *J. Am. Chem. Soc.* **2011**, *133*, 3728–3731.
(55) J. A. Kelly, K. E. Shopsowitz, J. M. Ahn, W. Y. Hamad and M. J. MacLachlan, *Langmuir* **2012**, *28*, 17256–17262.
(56) A. Querejeta-Fernández, G. Chauve, M. Methot, J. Bouchard and E. Kumacheva, *J. Am. Chem. Soc.* **2014**, *136*, 4788–4793.
(57) Z. Li, Z. Zhu, W. Liu, Y. Zhou, B. Han, Y. Gao and Z. Tang, *J. Am. Chem. Soc.* **2012**, *134*, 3322–3325.
(58) M. Schlesinger, M. Giese, L. K. Blusch, W. Y. Hamad and M. J. MacLachlan, *Chem. Commun.* **2015**, *51*, 530–533.

Table of Contents Entry:

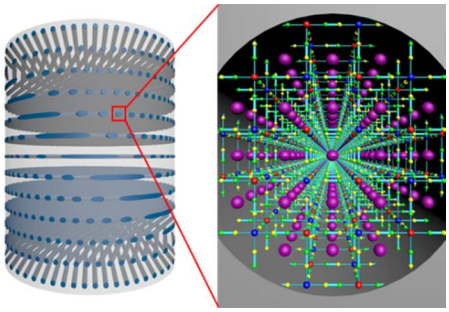

Prussian blue analogues with a chiral nematic superstructure have been prepared by hard templating inside chiral nematic mesoporous silica.